Design, Implementation and Validation of the KOMPSAT Spacecraft Simulator

Wan Sik Choi*, Sanguk Lee and Jong Won Eun*****
Satellite Communication System Department,
ETRI Radio & Broadcasting Lab.,Taejon, Korea
Han Jun Choi****
Precision Sensor & Satellite R&D Team,
DAEWOO Heavy Industries Ltd., Yongin, Korea
Dong Suk Chae****
System Development Section, Space Research Center,
Korea Aerospace Industries, LTD., Seosan Korea

Abstract

The spacecraft simulator is used for command validation, operational check of the Satellite Operation Subsystem (SOS), spacecraft anomaly analysis support, satellite operator training etc. In this paper, S/W design features and modeling characteristics of the KOMPSAT Spacecraft Simulator Subsystem (SIM) are described. Validation procedures and simulation results are also provided. The SIM provides extensive simulation capabilities by including models for most of the spacecraft subsystems. The software structure of the SIM was designed and implemented so as to support operations not only in real-time but also in non real-time by utilizing the Hewlett Packard (HP) UNIX functions. The SIM incorporates as many user-friendly Man Machine Interface (MMI) windows as possible so that all the SIM normal operations can be executed through the MMI windows.

Key Word : Satellite Simulator, AOCS, EPS, Spacecraft Model, MMI, KOMPSAT

Introduction

The KOMPSAT spacecraft simulator (SIM) is a comprehensive application software system which includes spacecraft subsystem mathematical models for the simulation of the KOMPSAT.

Major functions of the SIM are the validation of command, functional validation and operational check of the SOS, training of the KOMPSAT operators, anomaly analysis support, functional validation of the on-board flight software, and validation of spacecraft control laws and mission scenario, etc.

The KOMPSAT simulator, namely the SIM, provides real-time simulation capabilities for AOCS, EPS, TC&R and Ground Antenna Ranging & Tracking. DFVLR/GSOC developed the low Earth orbit spacecraft simulator for the ROSAT, so called AMCS simulator, which is mainly for AOCS simulation [1].

* Principal Member of Research Staff
Tel 82-42-860-5610, **Fax** 82-42-860-6949, **e-mail** choiws@etri.re.kr
** Senior Member of Research Staff
*** Principal Member of Research Staff, Team Leader
**** Assistant Research Engineer Chief
Tel 82-31-330-7750, **Fax** 82-31-330-7739, **e-mail** aeroman@iae.re.kr
Tel 82-42-860-2974, **Fax** 82-42-860-2977, **e-mail** dschae@xmail.kari.re.kr

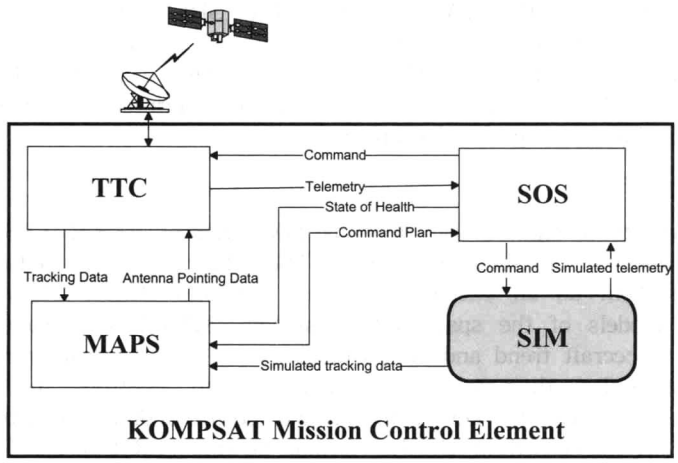

Fig. 1. Schematics of the KOMPSAT Mission Control Element

Italian Space Agency developed a geosynchronous satellite simulator, called the IAFSIM, which is also used mainly for simulation of spacecraft AOCS [3]. The SIM provides extensive simulation capabilities in the sense that it includes models for AOCS as well as EPS. The SIM also provides TC&R static simulation capability, i. e. telecommand and telemetry processing functions.

The KOMPSAT, which was launched in December 1999, is in a sun-synchronous orbit with an altitude of 685 km, eccentricity of 0.001, inclination of 98 deg and local time of ascending node of 10:50 a.m. The MCE [Fig. 1], the major ground station for the KOMPSAT, is being operated successfully for commanding the KOMPSAT through telecommand and telemetry.

In this paper, we describe the S/W design as well as operating features of the simulator, i.e. S/W structure and hierarchy, processing structure, and data exchange mechanism etc. Modeling details of the simulator such as orbit model, attitude dynamics model, various actuator models, disturbance torque models, and electrical power system models are also given in detail. Validation procedures of the simulator, i.e. the SIM test procedures are given by describing various levels of tests. Spacecraft anomaly analysis capability is also shown using the simulated anomaly case of the KOMPSAT.

SIM Structure

H/W Structure

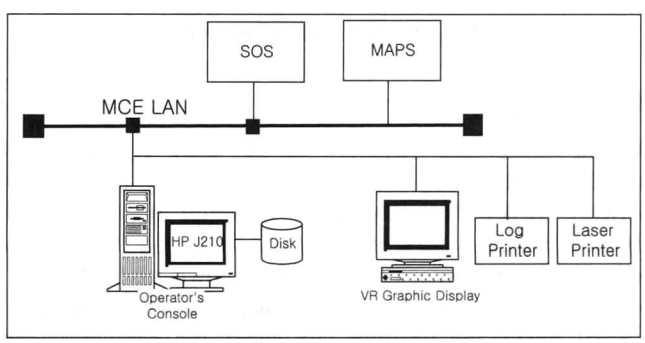

Fig. 2. SIM H/W Structure

Figure 2 shows the SIM H/W structure. The SIM main computer is the HPJ210 workstation which communicates with the other MCE subsystem, i.e. SOS and MAPS using the TCP/IP protocol via MCE LAN. The SIM also utilizes a pentium PC for VR graphic display of the KOMPSAT attitude and orbit motion. Two printers are used for printing out simulation results including images and graphics.

S/W Structure

The SIM consists of eight blocks such as MMI, Kernel, TC&R, EPS, Flight Dynamics, AOCS, Propulsion and Ground Simulation [Fig.3]. These blocks are grouped or divided as tasks in order to make them as an execution unit of the SIM. Under blocks, there are units containing mainly models of the spacecraft subsystem. MMI block handles command input, telemetry display, spacecraft trend and status display, etc. Kernel block processes telecommand and telemetry, schedules the tasks in real-time, and controls the simulation mode. Telecommand received from the kernel block, and corresponding telemetry generated from spacecraft models are processed in CCSDS format at the TC&R block. EPS block contains models for the simulation of electric power generation, battery status, and power system control unit. Blocks such as Flight Dynamics, AOCS and Propulsion are grouped as the sim_sdc task, which includes models for KOMPSAT orbit and attitude dynamics, sensors, actuators, and RDU. Ground simulation block contains models for tracking and ranging capabilities of the ground antenna.

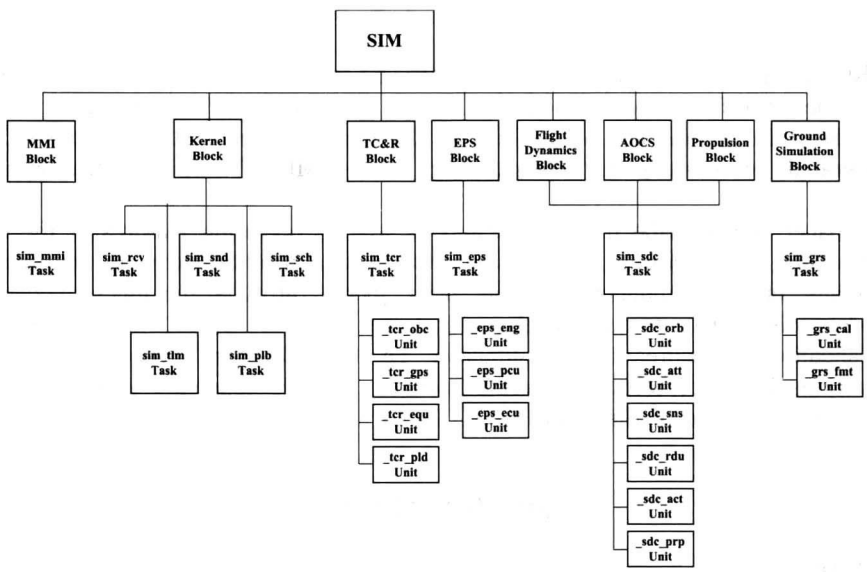

Fig. 3. SIM S/W Hierarchy

Processing Structure

Figure 4 shows the processing structure of the SIM. By the operator login from the **mmi**, the SIM is started, and the tasks are generated by using the HP UNIX system call. For message transfer between tasks, the SIM uses message queue and shared memory data structure. Message queue structures such as Msg_TC and Msg_TM are used for telecommand and telemetry processing. Shared memory structure[4] shown as SIM_COM (Fig. 4) is used for data communication of the simulation results which do not belong to telecommand and telemetry. From the MMI menu, the operator can select the simulator operation mode, namely SOS connection mode or stand-alone mode. The SIM can also be operated either in real-time

mode or non real-time mode. The **rcv** task of the kernel receives CCSDS formatted telecommand, and control command from the SOS, and routes the corresponding message to each task. The **snd** task of the kernel reads telemetry from the msg_TM. This task transmits the telemetry frame packet in CCSDS format and control response to the SOS. The **mmi** task manages the interface with the operator through the SIM main console and VR display. The **sch** task has a real-time scheduler function which does periodic requests every quarter second. It also analyzes real-time control command, changes parameters and flags, and transfers scheduler command to the tasks. The task execution sequence of the SIM is **sch** task, **tcr** task, **sdc** task, and **eps** task (refer to thick arrow line in Fig.4).

The KOMPSAT flight software is contained in three onboard processors, i.e. OBC for TM/TC processing , RDU for AOCS logic processing and ECU for EPS logic processing. In SIM, they are functionally modeled and embedded in three different tasks such as **tcr** for OBC, **sdc** for RDU and **eps** for ECU. In each of the tasks, flight software is interfaced with the spacecraft subsystem models[5], and does the same function as in onboard such as H/W data collection and command execution etc. Telemetry packets are generated from the flight software, and transmitted to the MCE SOS and the SIM MMI. Command packets received from the SOS and the SIM MMI are executed in the flight software.

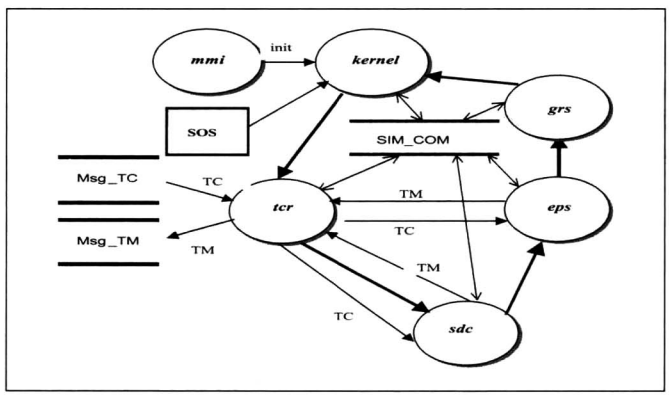

Fig. 4. SIM Processing Structure

Modeling Details

AOCS Model

In order to satisfy the real-time simulation requirement, i.e. quarter second simulation cycle constraint, models involving complexities such as attitude and orbit dynamics models need to be simplified forms. In the SIM, flags provided by the MMI window are used to adjust modeling complexities of the AOCS, and also to support selective anomaly simulation capabilities. By this, full models can be selected for off-line simulation, whereas simplified models for real time operation.

1) Orbit Model [6,7,10,11]

Orbit model is based on Keplerian orbit of two body problem, which can selectively include perturbations due to geopotentials up to 20 by 20 order in GEM9, Sun and Moon gravities, air drag using the MSIS model and H-P model, and solar radiation pressure.

$$\ddot{\underline{r}} = -\frac{\mu}{r^3}\underline{r} + \underline{P}_g + \underline{P}_s + \underline{P}_m + \underline{P}_u + \underline{P}_{srp} + u_{thruster} \tag{1}$$

where

$\underline{P}_g$: perturbation due to the mass distribution of the Earth.

$\underline{P}_s$, $\underline{P}_m$: Perturbation due to the gravitational effect by Sun and Moon, respectively.

$$\underline{P}_s = Gm_s\left(\frac{\underline{r}_s - \underline{r}}{\| \underline{r}_s - \underline{r} \|^3} - \frac{\underline{r}_s}{r_s^3}\right) \tag{2}$$

$$\underline{P}_m = Gm_s\left(\frac{\underline{r}_m - \underline{r}}{\| \underline{r}_m - \underline{r} \|^3} - \frac{\underline{r}_m}{r_m^3}\right) \tag{3}$$

where

m_s, m_m : mass of Sun and Moon

$\underline{r}_s$, $\underline{r}_m$, $\underline{r}$: position vector from the Earth to the Sun, the Moon and the spacecraft

$\underline{P}_a$: perturbations due to air drag effect

$$\underline{P}_a = -\rho\left(\frac{C_D A}{2m}\right)|\underline{v}_a|[v_{ax} \; v_{ay} \; v_{az}]^T \tag{4}$$

where

$\underline{v}_a = [\dot{x} + \omega_e y \;\; \dot{y} - \omega_e x \;\; z]^T$: velocity of the atmosphere near the satellite assuming corotating atmosphere.

ω_e : angular velocity of the Earth

C_D : drag coefficient

A : cross sectional area perpendicular to the direction of motion

m : spacecraft mass

ρ : atmospheric density at spacecraft altitude (using the MSIS model or H-P model)

$\underline{P}_{srp}$: perturbation due to solar radiation pressure.

$$\underline{P}_{srp} = KP_s \frac{S(\underline{r} - \underline{r}_s)}{m|\underline{r} - \underline{r}_s|} \times \mathrm{ECL}_{\mathrm{TYPE}} \tag{5}$$

where

$P_s = \frac{I_s}{c} = 4.5 \times 10^{-6} \; N/m^2$ at 1AU

S : cross sectional area of the satellite as constant value,

m : satellite mass,

$\underline{r}_s$: position vector from the Earth to the Sun,

$\underline{r}$: position vector from the Earth to the spacecraft,

K : reflection factor of the satellite surface

(K : 1.95 for aluminum, 1 for black body, 2 for total reflection)

$\mathrm{ECL}_{\mathrm{TYPE}}$: Eclipse Type (0.0 for Eclipse, 1.0 for Sun Light)

2) Attitude Model [6,7,8,9]

For the attitude dynamics of the KOMPSAT, the rigid body dynamics of the spacecraft are modeled by the Euler moment equation, and the flexibility of the solar arrays and its beam are also modeled by using assumed mode method and multibody dynamics. Changes of moments of inertia and center of gravity of spacecraft due to solar array rotation and fuel consumption are also included in attitude model. Environmental disturbance torque due to gravity gradient, aerodynamic drag, solar radiation pressure and residual magnetism are also included in the attitude dynamics. Detailed derivation of the equations in this paper are described in reference [12].

Let $\underline{H} = I\underline{\omega} + \underline{H}_W$ be the total angular momentum of the KOMPSAT, i.e. sum of angular momentum of the spacecraft and that of the reaction wheel. Then the rigid body dynamics of the KOMPSAT take the following Euler equation.

$$I\dot{\underline{\omega}} + \dot{\underline{H}}_W + \underline{\omega} \times (I\underline{\omega} + \underline{H}_W) = \underline{T} \tag{6}$$

where

$$I=\begin{bmatrix} I_{xx} & I_{xy} & I_{xz} \\ I_{yx} & I_{yy} & I_{yz} \\ I_{zx} & I_{zy} & I_{zz} \end{bmatrix}$$

$\underline{\omega}=[\omega_x\ \omega_y\ \omega_z]^T$

$\underline{H}_W=[H_{Wx}\ H_{Wy}\ H_{Wz}]^T$

$\underline{T}=[T_x\ T_y\ T_z]^T$: sum of disturbance torque and actuator control torque w.r.t. BFC.

Quaternion is updated by the following kinematic equation using the angular velocities obtained from (6).

$$\frac{d\underline{q}}{dt}=\frac{1}{2}\Omega\underline{q} \tag{7}$$

where

$$\Omega=\begin{bmatrix} 0 & \omega_z & -\omega_y & \omega_x \\ -\omega_z & 0 & \omega_x & \omega_y \\ \omega_y & -\omega_x & 0 & \omega_z \\ -\omega_x & -\omega_y & -\omega_z & 0 \end{bmatrix}$$

$\underline{q}=[q_1\ q_2\ q_3\ q_4]^T$

3) Environmental Torque Model

Aerodynamic Torque

In order to calculate the aerodynamic torque, KOMPSAT configuration is approximated by six plates and one cylinder, i.e. two plates for each solar panel, two plates for top and bottom of the main body, and one cylinder for the main body. Total aerodynamic torque acting on the spacecraft w.r.t. BFC is obtained by summing the moments on each plate and cylinder.

$$\underline{T}_a=\sum_i \underline{R}_{plate,i}\times \underline{F}_{plate,i} + \underline{R}_{cylinder}\times \underline{F}_{cylinder} + \underline{M}_{cylinder} \tag{8}$$

where

$\underline{R}_{plate,i}$: moment arm vector from the origin of the BFC to center of mass of the plate,i

$\underline{R}_{cylinder}$: moment arm vector from the origin of the BFC to center of mass of the cylinder

Aerodynamic force acting on a plate :

$$\underline{F}_{Plate}=2qA\cos\eta_p\{f_T\,\underline{\delta}_F+(2-f_N-f_T)\cos\eta_p\,\hat{\underline{n}}_p\},\ (\cos\eta_p>0) \tag{9}$$

Aerodynamic force and torque acting on the cylinder :

$$\underline{F}_{cylinder}=\frac{4}{3}qLD\sin\eta_c\{(2+0.5\,f_T-f_N)\,\underline{\delta}_F+(2-f_N-f_T)\cos\eta_c\,\underline{\delta}_c\} \tag{10}$$

$$\underline{M}_{cylinder}=\frac{\pi}{4}qLD^2f_T\sin\eta_c(\underline{\delta}_F\times\underline{\delta}_c) \tag{11}$$

where

A : area of a plate

q : Dynamic pressure

f_T : Tangential accommodation coefficient

f_N : Normal accommodation coefficient

$\hat{\underline{n}}_p$: inward unit vector normal to the plate.

$\eta_p=\cos^{-1}(\hat{\underline{n}}_p\cdot\hat{\underline{\delta}}_c)$

L, D : height and diameter of cylinder

$\hat{\underline{\delta}}_c$: unit vector along cylinder longitudinal axis

$\eta_c=\cos^{-1}(\hat{\underline{\delta}}_c\cdot\hat{\underline{\delta}}_F)$

$\hat{\underline{\delta}}_F = -\hat{\underline{i}}_{LVLH}$

$\hat{1}_{LVLH}$: unit vector along the X-axis in the LVLH coordinate system.

Magnetic Disturbance Torque

Torque due to the interaction between residual magnetism of the spacecraft and Earth's magnetic field can be calculated as follows.

$$\underline{T}_M = \underline{M} \times \underline{B} \tag{12}$$

where

$\underline{M}$: residual magnetic field of the spacecraft w.r.t. BFC obtained from the vendor data

$\underline{B}$: geomagnetic field vector w.r.t. BFC, calculated from IGRF model or dipole model

Gravity Gradient Disturbance Torque

Gravity gradient disturbance torque can be calculated by the following equations about BFC.

$$\begin{aligned} T_{gx} &= 3\omega_0^2\{(I_{zz}-I_{yy})C_{23}C_{33} - I_{yz}(C_{23}^2 - C_{33}^2) + I_{xy}C_{13}C_{33} - I_{xz}C_{13}C_{23}\} \\ T_{gy} &= 3\omega_0^2\{(I_{xx}-I_{zz})C_{13}C_{33} + I_{xz}(C_{13}^2 - C_{33}^2) + I_{yz}C_{13}C_{23} - I_{xy}C_{23}C_{33}\} \\ T_{gz} &= 3\omega_0^2\{(I_{yy}-I_{xx})C_{13}C_{23} + I_{xy}(C_{23}^2 - C_{33}^2) + I_{xz}C_{23}C_{33} - I_{yz}C_{13}C_{33}\} \end{aligned} \tag{13}$$

where

C_{ij} : element of direction cosine matrix from ECI to BFC

ω_0 : orbital rate

I_{ij} : moment of inertia tensor

Solar Radiation Pressure Disturbance Torque

Torque due to solar radiation pressure w.r.t. the BFC:

$$\underline{T}_s = \sum_i \underline{R}_{plate,i} \times \underline{F}_{plate,j} + \underline{R}_{cylinder} \times \underline{F}_{cylinder} + \underline{M}_{cylinder} \tag{14}$$

Solar radiation force on an arbitrary plate :

$$\underline{F}_s = V_s A \cos\eta_p \{(1-\nu_T)\,\hat{\delta}_F + (\nu_N+\nu_T)\cos\eta_p\,\hat{n}_p\}, \ (\cos\eta_p > 0) \tag{15}$$

$$\underline{F}_{plate} = \underline{0}, \ (\cos\eta_p < 0)$$

Solar radiation force and torque on the cylinder :

$$\underline{F}_{cylinder} = \frac{2}{3} V_s L D \sin\eta_c \{(\frac{3}{2} + \nu_N - 0.5\nu_T)\,\hat{\delta}_F - (\nu_N+\nu_T)\cos\eta_c\,\hat{\delta}_c\} \tag{16}$$

$$\underline{M}_{cylinder} = \frac{\pi}{8} V_s L D^2 (1-\nu_T)\cos\eta_c (\hat{\delta}_F \times \hat{\delta}_c) \tag{17}$$

where

V_s : solar pressure constant

A : surface area of the plate

q : dynamic pressure

ν_T : tangential accommodation coefficient

ν_N : normal accommodation coefficient

$\hat{n}_p$: inward unit vector normal to flat plate

$\eta_p = \cos^{-1}(\hat{n}_p \cdot \hat{\delta}_F)$

L : height of cylinder

D : diameter of cylinder

$\hat{\delta}_c$: unit vector along cylinder longitudinal axis

$\eta_c = \cos^{-1}(\hat{\delta}_c \cdot \hat{\delta}_F)$

$\hat{S}$: unit Sun vector

$\hat{\delta}_F = -\hat{S}$

4) Actuator Model

Reaction Wheel

Four reaction wheels are installed in inverted pyramid form with respect to the x-y plane such that components of each wheel angular momentum are same for all three body axes.

$$\begin{bmatrix} H_{wx} \\ H_{wy} \\ H_{wz} \end{bmatrix} = \begin{bmatrix} k\cos\theta & -k\cos\theta & -k\cos\theta & k\cos\theta \\ k\cos\theta & k\cos\theta & -k\cos\theta & k\cos\theta \\ \sin\theta & \sin\theta & \sin\theta & \sin\theta \end{bmatrix} \begin{bmatrix} H_{w1} \\ H_{w2} \\ H_{w3} \\ H_{w4} \end{bmatrix} \tag{18}$$

where

$k = \cos 45^o$

θ : fixed value satisfying the above condition for reaction wheel installation

H_{wx}, H_{wy}, H_{wz} : angular momentum of reaction wheel assembly in BFC.

H_{w1}, H_{w2}, H_{w3}, H_{w4} : angular momentum of each wheel.

Wheel torque can be represented as the sum of the wheel motor torque and its friction torque.

$$\underline{T}_w = \underline{T}_m - \underline{T}_f \tag{19}$$

where

$\underline{T}_w$: wheel torque,

$\underline{T}_m$: wheel motor torque,

$\underline{T}_f$: wheel friction torque, obtained from the lookup table from the vendor.

Angular velocity and momentum of the reaction wheel assembly are obtained by the numerical integration of the following differential equation.

$$I_w \ddot{\theta}_w = \underline{T}_w \tag{20}$$

where

θ_w rotating angle of wheel w.r.t. BFC frame and $I \gg I_w$.

Magnetic Torquer

Magnetic torquer is modeled to generate torque according to the on-time and polarity command signal. Torque generated by the magnetic torquer can be obtained by the following equation.

$$\underline{T}_M = \sum_{i=1}^{3} (\underline{M}_i \times \underline{B} + \underline{M}_{residual,i} \times \underline{B}) \tag{21}$$

where

$\underline{M}_i$: magnetic moment vector of the torque

$\underline{M}_{residual,i}$: residual magnetic moment of the tprque

$\underline{B}$: Earth's magnetic field obtained from the IGRF.

Thruster Torque

Torque generated due to thruster firing is obtained by the following equation.

$$\underline{T}_{TH} = \sum_{i=1}^{4} (\underline{R}_i - \underline{R}_{CG}) \times \underline{F}_i \tag{22}$$

where

$\underline{R}_i$: position vector of the thruster w.r.t. the satellite separation point

$\underline{R}_{CG}$: position vector of the center of mass of the KOMPSAT w.r.t the separation point

$\underline{F}_i$: thrust force vector due to ith thruster firing.

Fuel consumption and fuel tank pressure are also considered in the calculation of the thruster torque.

Solar Array Drive

Solar array drive model calculates the rotation angles of the two solar arrays according to command word from RDU model. Then solar array rotation angles are sent to the attitude model, environmental torque model and EPS model to calculate the changes of moments of inertia, aerodynamic and solar radiation pressure torque, and electrical characteristics.

5) Sensor Model

Sensors used for AOCS, i.e. GRA, CSSA, FSSA, CES, Potentiometer, Tachometer and TAM are modeled by referencing the manufacturers data.

GRA is modeled to generate counts representing incremental angles of S/C for all six GRAs.

The counts generated by the GRA can be obtained by the following equation.

$$\underline{\theta} = A^T(\underline{W} + \underline{D})\triangle T + N \tag{23}$$

$$C_i = \theta_i / K_{GRA,i} \tag{24}$$

where

$\underline{\theta}$: Incremental Angle in Body Fixed Frame
A : Body to GRA Transformation Matrix
$\underline{W}$: Body Rates
$\underline{D}$: Drift Rates
$\triangle T$: Sampling Time
$\underline{N}$: Noise
$\underline{C}$: Gyro Output Counts
$K_{GRA,i}$: Scale Factor for GRAs.

CSSA is modeled to generate counts representing output current from four CSSs. The counts generated by the CSSA can be obtained by the following equation.

$$i_{Cel} = i_{Max} \cos\theta \times \mathrm{ECL}_{\mathrm{TYPE}} + \underline{B} + \underline{N} \tag{25}$$

$$C_i = i_{Cel,i} / K_{CSS,i} \tag{26}$$

where

$\underline{C}$: CSSA Output Counts
i_{Max} : Maximum Current for Each Cell
i_{Cel} : Each Cell Current
θ : Sun Incident Angle in CSS Axis
$\mathrm{ECL}_{\mathrm{TYPE}}$: Eclipse Type
$\underline{B}$, $\underline{N}$: Bias, Noise
$\underline{K}_{CSS,i}$: Scale Factor for CSSs

FSSA is modeled to generate counts representing output current from the three cells of each of two sun sensors. The counts generated by the FSSA can be obtained by the following equation.

$$i_{Cel} = i_{Tab}\, S \times \mathrm{ECL}_{\mathrm{TYPE}} + \underline{B} + \underline{N} \tag{27}$$

$$C_i = i_{Cel,i} / K_{FSS,i} \tag{28}$$

where

$\underline{C}$: FSSA Output Counts
i_{Tab} : Table Value of Each Cell Current by Sun Incident (Azimuth) Angle
$i_{Cel,i}$: Each Cell Current
E : Eclipse Type
S : Shading Effect
$\underline{B}$, $\underline{N}$: Bias, Noise
K_{FSS} : Scale Factor

CES is modeled to generate counts representing the horizon crossing angle for two conical earth sensors. Angle generated by the CES can be obtained by the following equation for spherical earth model. The effect for the earth oblateness and radiance is also included.

$$V=\tan^{-1}\frac{U_1}{U_2}\pm\frac{\cos\alpha-\cos\beta\times U_2^2}{\sin\beta\sqrt{1-U_2^2}} \tag{29}$$

where

$\pi-V_1$: The angle between TDC (Top Dead Center) and LE (Leading Edge)

$\pi-V_2$: The angle between TDC (Top Dead Center) and TE (Tailing Edge)

U_1, U_2, U_3 : Nadir Unit Vector in CES Axis

α: Earth Half Cone Angle

β: CES Scan Cone Half Apex Angle

TAM is modeled to generate counts representing the output voltage for two TAMs. The voltage generated by the TAM can be obtained by the following equation.

$$C_i=(A^T\underline{H}+\underline{B}+\underline{N})_i/\ K_{TAM,i} \tag{30}$$

where

$\underline{C}$: TAM Output Counts

A : Body to TAM Transformation Matrix

$\underline{H}$: Magnetic Field Vector in Body Axis

$K_{TAM,i}$: Scale Factor

$\underline{B}$, $\underline{N}$: Bias, Noise

Tachometer is modeled to generate counts representing the wheel speed for four tachometers. Potentiometer is modeled to generate counts representing the solar array angle for four solar array potentiometer.

EPS model

EPS model comprises three units of ENG, PCU and ECU. ENG unit consists of solar array model for electricity generation, SAR model for regulation of electricity generation, DDC model for deployment status of solar array panel. PCU consists of control logic model for electricity supply, battery model for charging capacity, battery efficiency and battery voltage due to various conditions. ECU consists of sensor data processing model and charging mode algorithm functionally modified from on-board flight software [5]. Models for solar array power generation and battery are obtained using the data generated from the neural network algorithm [Fig. 5, Table 1,2,3,4].

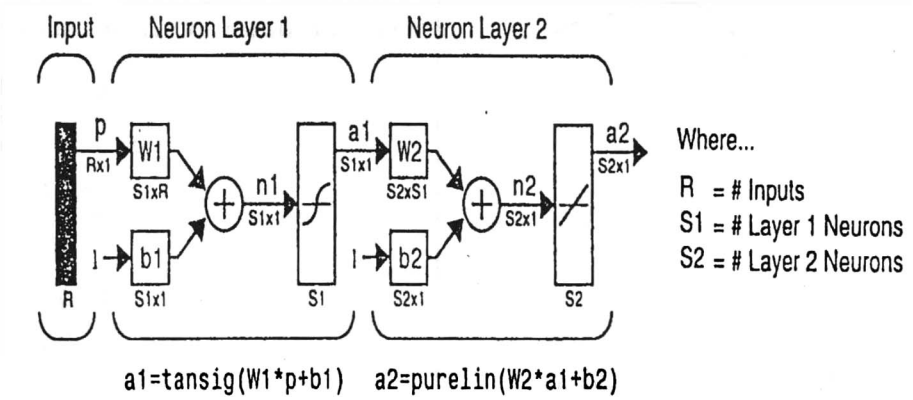

Fig. 5. Neural Algorithm for EPS Modeling

1) Solar Array Model

Solar array of KOMPSAT is designed to provide at least 560Watts power at the end of its lifetime and its component configuration is shown in Table 1.

Solar array is modeled based on the current vs voltage curve and power decay due to its aging effects and temperature variations is also reflected[Fig. 6]. Figure 6 shows solar array output power degradation due to its aging effects. Empirical data of current and voltage curve for solar array are shown in Figure 7.

Table 1. Neural Model of Solar Array w. r. t. Time and Output Voltage at 28 degrees.

Components	Number	Components	Number
Wing	2	Panels/Wing	2
Panels	10	Strings/Panel	4
Strings	40	Cells/String	107

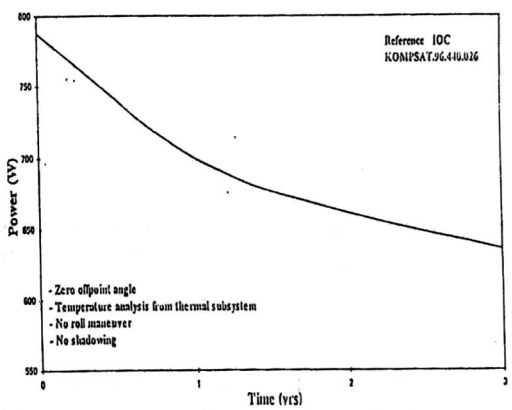

Fig. 6. Solar Array Output Degradation due to Aging Effects.

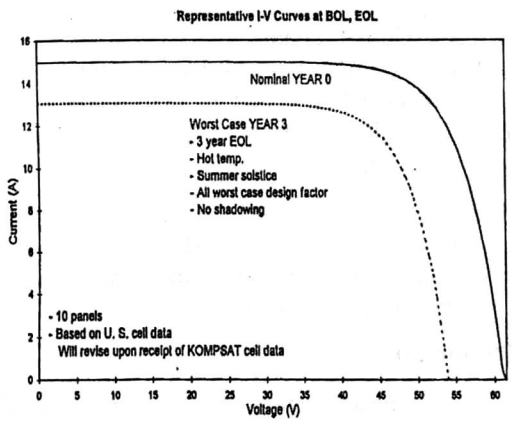

Fig. 7. Solar Array Current-Voltage Curve at the BOL and the EOL of Satellite

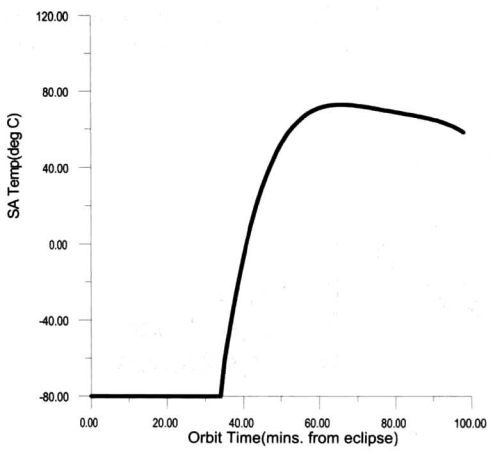

Fig. 8. Solar Array Temperature during One Orbit Period.

Table 2. Neural Model of Solar Array w. r. t. Time and Output Voltage at 28 degrees.

Neural Coefficient	Current (Ampere)
W1	0.1253, - 10.7419 - 0.1189, - 0.1629 0.0013, - 0.5766
W2	1365.7 2067.8 - 6.2
b1	- 10.7047 9.9010 1.3054
b2	- 681.717

According to empirical data shown on figures 6 through 8, neural models for variations of solar array output currents and voltages due to aging were developed and shown in Table 2.

Figure 9 shows 3D Solar Array Current-Voltage Curve for KOMPSAT Lifetime at the temperature of 28 degrees using neural network model shown in Table 1.

Open circuit voltage for solar array decreases at rate 0.0021 V/Deg C, and this factor is applied to the solar array model.

2) Battery Model

Super Ni-Cd Battery for KOMPSAT is composed of 22 cells and its capacity is 21 AH. Charge and discharge models of battery were developed as shown in table 3 and 4, respectively. Charge and discharge efficiencies have also considered [Fig. 10].

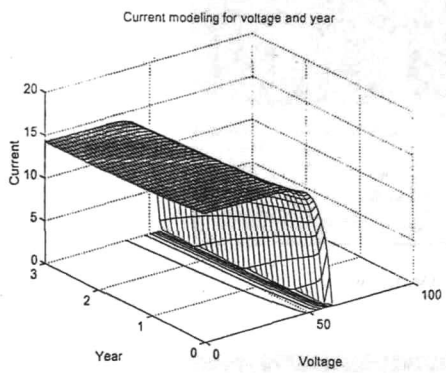

Fig. 9. Solar Array Current-Voltage Curve for KOMPSAT Lifetime at 28 deg C.

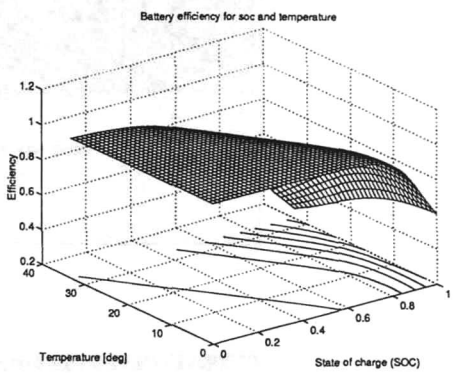

Fig. 10. Solar Array Current-Voltage Curve for KOMPSAT Lifetime at 28 deg C.

Table 3. Neural Model of Battery Charge Voltage w.r.t. AH ratio.

Neural Coefficient	Neural Model of Battery Charge Voltage
W1	-86.3790, -0.6804
W2	-0.0937, -4.3233
b1	1.7123, 2.8764
b2	4.5838

Table 4. Neural Model of Battery Discharge Voltage w.r.t. AH ratio.

Neural Coefficient	Neural Model of Battery Discharge Voltage
W1	119.6921, -4.9835, 4.1392
W2	-0.5148, 3.7011, -5.2287
b1	-122.2251, 6.7686, 2.2728
b2	2.2023

TC&R model

TC&R model comprises four units, i.e. OBC, GPS, EQU and PLD. OBC unit includes processing logic of command and telemetry. It also models the status of the OBC, 1553B bus and watch dog timer. GPS unit models the status of the equipment, and provides data for time, position and velocity. EQU and PLD units model the status of various payload equipment.

MMI Development

SIM is designed and developed such that all the operation can be managed through the MMI window. Thus command input, telemetry display, and spacecraft trend and status display, etc can be done using the user friendly designed MMI windows. Figures 11 and 12 are a few

examples of the MMI windows implemented in the SIM. Figure 11 shows ground track display of the KOMPSAT, and it also shows if the satellite contacts with the ground station. Figure 12 is the MMI window for celestial track which shows the locations of Earth, Sun, and Moon on the 2D transformation plane of 3D celestial sphere w.r.t. the KOMPSAT. It also shows if the Earth and Sun are in the FOV of the CES and FSS respectively.

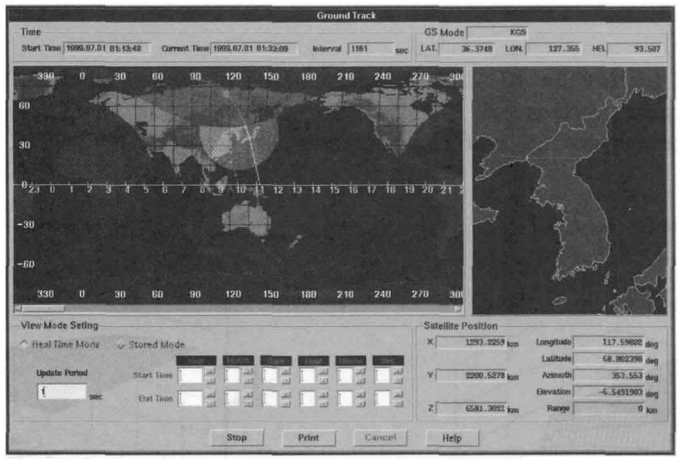

Fig. 11. Ground Track Window

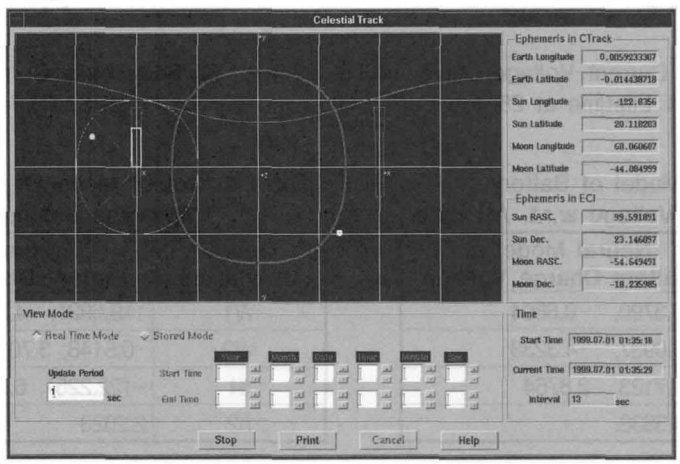

Fig. 12. Celestial Track

SIM Validation

Validation Procedures

SIM is validated through various levels of tests [Fig.13]. As shown in Fig. 13, SIM Test comprises Function Test, Task Test, Integration & Test and Acceptance Test. Function level tests are carried out by the responsible engineer, and test reports are generated and reviewed. Task (an execution unit of the SIM) was tested by using the test program prepared by the related responsible engineers. Test programs were devised so that they can be executed independently with other tasks.

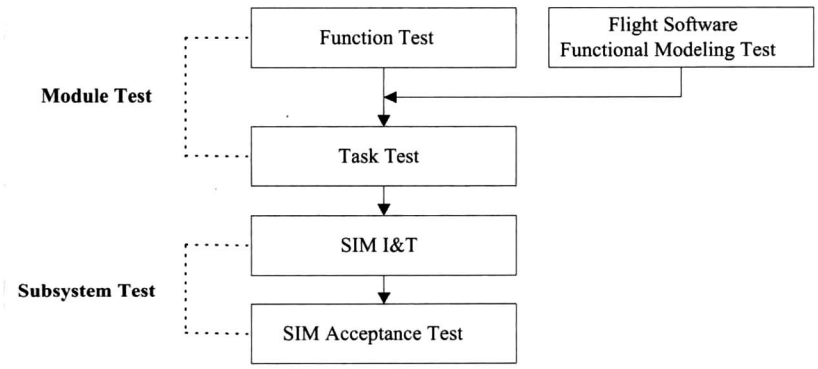

Fig. 13. SIM Validation Procedures

SIM I&T was carried out with all the SIM tasks are integrated, and in this phase of test, the SIM integrated functional and performance capabilities were checked through the MMI by the test team. SIM test procedures were prepared such that all the requirements were traceable and complied to the SIM specification. Test environments were constructed similarly to the SIM H/W structure [Fig. 2], and test harnesses were prepared for the interface tests with other MCE subsystems, i.e. SOS, MAPS.

Test Details

Test items described in the SIM test procedure can be classified as four major functional groups such as SIM Management, TC/TM Processing, MMI Processing and Spacecraft Modeling.

SIM Management comprises test items such as security check for the termination and start of the SIM, SIM Initialization, Simulation Mode, External Interface, SIM Time Synchronization using NTP, Data Storage Capability for 10 hours simulation, Minor cycle Execution Capability of Telecommand, Process Self Diagnosis, Print Out of Simulation Results.

TC/TM Processing, which is one of the most important SIM function in the sense that telecommands were validated through this capability, comprises test items such as Command Processing, (i.e. Real Time, Absolute Timed, and Relative Timed), TM Monitoring, SOH Collection and Monitoring. Typical TC/TM set was selected in order to check the processing capability of this test. Test program was used to check the complete TC/TM set.

SIM has to be designed and developed to have use-friendly MMI in the sense that the user can operate the SIM in various cases through the MMI. Test items for the MMI were : Spacecraft Ground Track, Satellite in ECI, Sensor View, Equipment Status View, 3D Attitude Graphic Display utilizing Virtual Reality Tool.

SIM includes model for Attitude and Orbit Control Subsystem, Electrical Power Subsystem, TC&R Subsystem of the KOMPSAT. Test items for the SIM Models were : Orbit dynamics, Attitude Dynamics Model, Sensor Model, Attitude Determination, Reaction Wheel, Torque Rod, Solar Array, Battery Charge, Duty Ratio, GPS Equipment Status, Propulsion Model, GRS Simulation.

Simulation Results

Validation of the developed models has been performed through function tests and task tests. Figures 14a and 14b show the test results of orbit dynamics model. They shows the same trend for 20 by 20 order of geopotential model with that of the commercial tool such as OWB.

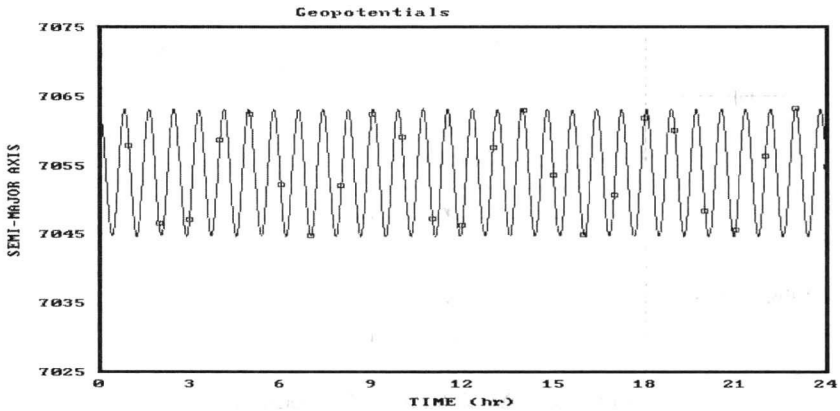

Fig. 14a. Time History of Semi-Major Axis by OWB

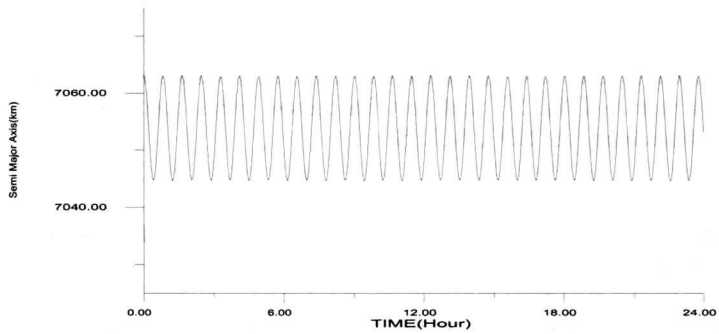

Fig. 14b. Time History of Semi-Major Axis by SIM

Figure 15 shows changes of moment of inertia of spacecraft due to solar array rotation as a result of attitude dynamics model test. Since the solar array is symmetric w.r.t. y-axis, no variation is observed for Iyy. But periodic variations of Ixx and Izz are observed. Ixx and Izz vary periodically as the solar arrays rotate, but Iyy does not vary because of the symmetric configuration of the solar arrays about y-axis. Figure 16 shows the spacecraft attitude variation due to 30 degree roll maneuver of science mode. It shows that the 300sec settling time requirement is satisfied, and the steady state response is stabilized. Figure 17 shows the simulation results when all the reaction wheels are operating normally under science mode. Spacecraft settles down to the LVLH frame, which shows the KOMPSAT specifications are satisfied; pointing error requirements are 0.1deg for roll, 0.18deg for pitch, and 0.5deg for yaw w.r.t LVLH.

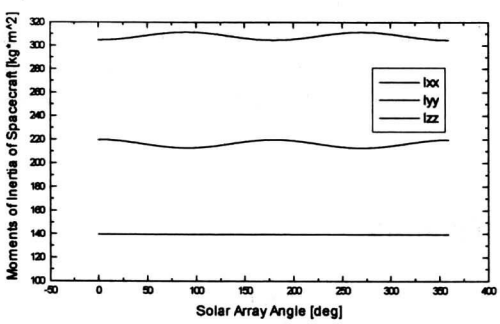

Fig. 15. The Changes of Moments of Inertia due to Solar Array Rotation

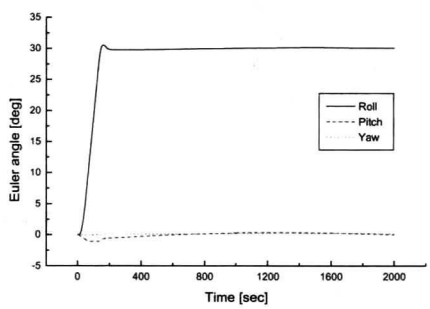

Fig. 16. Test Results of 30deg Roll Maneuver in Science Mode

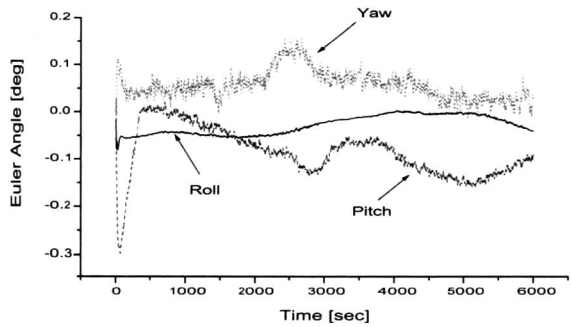

Fig. 17. Euler Angle referenced to LVLH in case of Normal Science Mode

Figures 18a and 18b show changes in body rates, and angle between solar array normal and Sun line in the sun point mode. It shows that the requirements are satisfied : angle between solar array normal and Sun line should be ≤ 10deg within 600sec, and maintain this state afterwards except the eclipse period, and steady state roll rate control error is ≤ 0.15 deg/sec. The time histories of solar array temperature, and solar array open circuit voltage, and battery charge and discharge currents for one orbit period in **eps** task are presented in Figures 18 and 19.

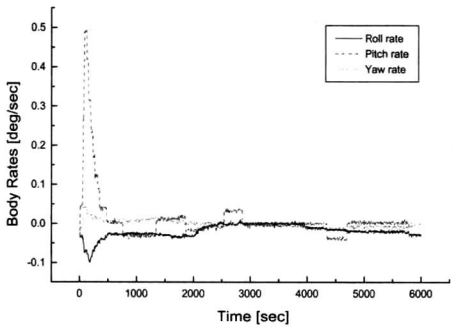

Fig. 18a. Body rates in Sun Pointing Mode

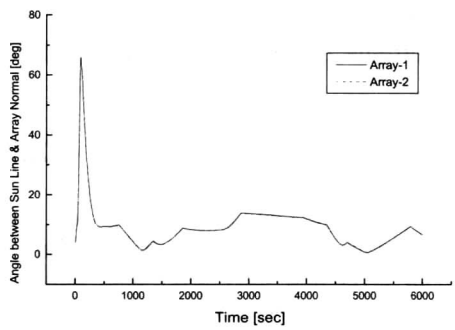

Fig. 18b. Angle between Array Normal and Sun Line in Sun Pointing Mode

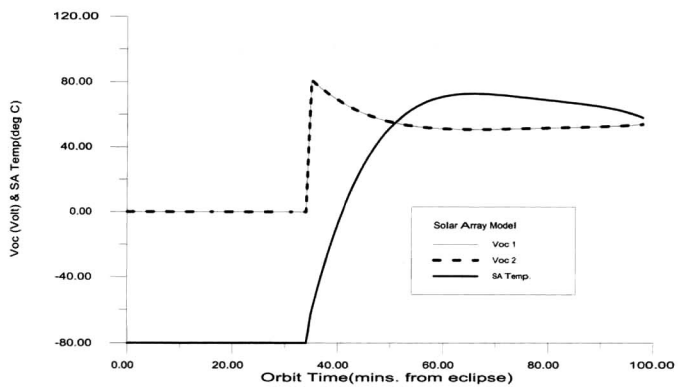

Fig. 19. Solar Array Temperature and Open Circuit Voltages during Eclipse and Sunlight

Figure 20 shows one of the SIM capabilities, i.e. spacecraft anomaly analysis capability. This figure shows the simulation results when reaction wheel-1 fails under science mode. After the anomaly on reaction wheel-1 initiated at 1000secs from the simulation start time, the spacecraft loses its control and begins to oscillate. Using these capabilities implemented in the SIM, various cases of spacecraft anomalies can be simulated as well as analyzed.

Processing capabilities of telecommand and telemetry are validated not only through the SIM MMI window but also using the SOS window, namely in the SOS connection mode. Simulation results observed through the MMI window show that minor cycle (0.25sec) execution requirement is satisfied, and all the telecommand and telemetry are processed correctly in the SIM.

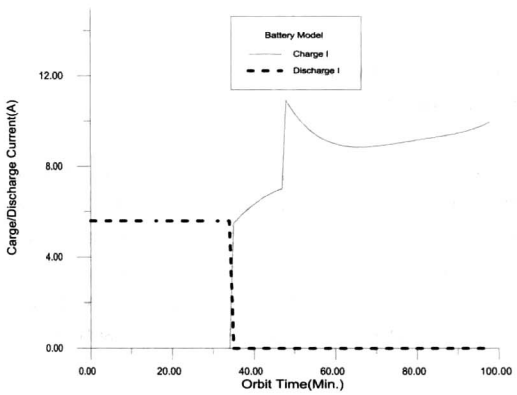

Fig. 20. Battery Charge and Discharge Currents During Eclipse and Sunlight.

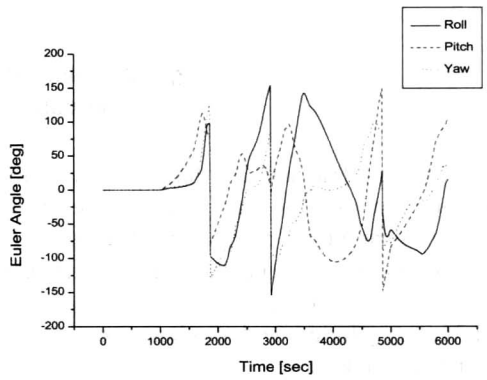

Fig. 21. Euler Angle referenced to LVLH in the case of Reaction Wheel 1 Failure

Conclusions

In this paper, design features and modeling characteristics of the KOMPSAT Spacecraft Simulator Subsystem (SIM) have been described. The SIM has been validated through functional level and task level test, and some of those simulation results are presented. The Man Machine Interface (MMI) development features of the SIM are also presented. One of the important SIM capabilities, namely spacecraft anomaly analysis capability is also shown using the simulated anomaly case.

Acknowledgements

The work presented in this paper had been funded by the Korea Ministry of Information and Communications. Special thanks also go to the Korea Aerospace Research Institute and the Ministry of Science and Technology for their supports in many respects.

References

1. User Manual, ROSAT AMCS Simulator, DFVLR/GSOC, March 1992.

2. J. Biesiadecki, D. Henriquez and A. Jain, "A Reusable, Real-Time Spacecraft Dynamics Simulator," in 6th Digital Avionics Systems Conference, (Irvine, CA), Oct 1997

3. A. Ramos, et al, Design and Validation of the ITALSAT AOCS flight simulator, COMSAT Technical Review Volume 23 Number 1, Spring 1993.

4. Ja-Young Kang, Jae-Moung Kim, and Seon Jong Chung, Design and Development of an Advanced Real-Time Satellite Simulator, Etri Journal, Vol. 17, No. 3, October 1995.

5. Sanguk Lee, Dong Suk Chae, and Wan Sik Choi, Implementation of Interface between Satellite Subsystem Model and Flight Software on KOMPSAT Simulator, Journal of The Korean Society for Aeronautical and Space Science, Vol. 27 , No. 3 , 1999.

6. James R. Wertz, Spacecraft Attitude Determination and Control, Kluwer Academic Publisher, 1988

7. James R. Wertz, Wiley J. Larson, Space Mission
Analysis and Design, Kluwer Academic Publisher, 1991

8. Marshall H. Kaplan, Modern Spacecraft Dynamics & Control, John Wiley & Sons, 1976

9. Roy R. Craig, Jr, Structural Dynamics : An Introduction to Computer Method, Wiley, 1981

10. Gunter Seeber, Satellite Geodesy : Foundation, Methods, and Applications, Walter de Gruyter, 1993

11. Richard H. Battin, An Introduction to The Mathematics and Methods of ASTRODYNAMICS, AIAA Education Series, AIAA, Inc., 1987

12. Sanguk Lee and Han Jun Choi, Flight Dynamic Modeling of KOMPSAT Simulator, Technical Memo, ETRI, 1997.

Acronyms & Abbreviations

AMCS	Attitude Measurement and Control Subsystem
AOCS	Attitude and Orbit Control Subsystem
AU	Astronomical Unit
BFC	Body Fixed Coordinate system
CAL	Calculation (SIM unit name)
CCSDS	Consultative Committee for Space Data System
CES	Conical Earth Sensor
CSS(A)	Coarse Sun Sensor (Assembly)
DDC	Deployment Device Controller
ECI	Earth Centered Inertial coordinate system
ECU	Electrical Control Unit
ENG	Energy Generation (SIM unit name)
EPS	Electrical Power Subsystem
EQU	Equipment (SIM unit name)
ETRI	Electronics and Telecommunications Research Institute
FOV	Field Of View
FSS(A)	Fine Sun Sensor (Assembly)
GPS	Global Positioning Satellite
GRA	Gyro Reference Assembly
GSOC	German Space Operation Center
H-P	Harris Priester
HP	Hewlett Packard
IAFSIM	ITALSAT AOCS Flight Simulator
IGRF	International Geomagnetic field Reference Field
KOMPSAT	KOrea Multi Purpose SATellite
LVLH	Local Vertical Local Horizontal coordinate system
MAPS	Mission Analysis and Planning Subsystem
MCE	Mission Control Element
MMI	Man Machine Interface
MSIS	Mass Spectrometer Incoherent Scatter
OBC	On Board Computer
OWB	Orbital Work Bench
PCU	Power Control Unit
PLD	SIM unit name
PC	Personal Computer
RDU	Remote Drive Unit
RWA	Reaction Wheel Assembly
SADA	Solar Array Drive Assembly
SIM	KOMPSAT Spacecraft SIMulator Subsystem
SOS	Satellite Operation Subsystem
TC	Telecommand
TC&R	Tracking, Command & Ranging Subsystem
TM	Telemetry
TAM	Three Axis Magnetometer
VR	Virtual Reality
w.r.t.	with respect to